

Air bubble formation and dissolution in dispensing nanoimprint lithography

Xiaogan Liang¹, Hua Tan², Zengli Fu¹ and Stephen Y Chou^{1,3}

¹ Nanostructure Laboratory, Department of Electrical Engineering, Princeton University, Princeton, NJ 08544, USA

² Nanonex Corporation, Monmouth Junction, NJ 08552, USA

E-mail: xliang@princeton.edu and chou@princeton.edu

Received 23 August 2006, in final form 2 November 2006

Published 15 December 2006

Online at stacks.iop.org/Nano/18/025303

Abstract

We report an experimental and theoretical study of two most critical yet still to-be-answered issues in dispensing-based nanoimprint lithography (D-NIL): air bubble formation and absorption, and discuss their impact on NIL yield and throughput. Using real-time observation via video, we found two different mechanisms for air bubble formation (feature pinning and multi-droplet encircling), and studied the dynamic behaviour of the air absorption and air bubble shrinking under different conditions. Furthermore, we developed theoretical models and simulation programs of the air absorption and bubble shrinking based on molecular diffusion theory and hydrodynamics. We compared these models with experiments, and found excellent agreement. Our study shows that the key factors that affect the air dissolution time (and hence the air bubble shrinking time) are air bubble initial size, imprinting pressure, air solubility, and resist residue layer thickness. One of our key conclusions from the study, which has significant practical importance, is that although the air in a bubble can be completely dissolved in a resist liquid as long as the bubble is smaller than a certain size, the air absorption time might be too long for the dispensing-NIL operating in atmosphere or poor vacuum to have a necessary throughput in mass manufacturing.

(Some figures in this article are in colour only in the electronic version)

1. Introduction

Nanoimprint lithography (NIL) has shown the capability of patterning structures smaller than 10 nm with a high throughput [1, 2]. One of the central goals in today's NIL research is to develop the methods that can improve NIL performance and yield, and to make NIL suitable for mass production. One of the NIL processes under current study is dispensing-based NIL (D-NIL), which generally describes a group of relevant and similar procedures using dispensed liquid resist including micromoulding in capillaries (MIMIC) [3], and step-and-flash imprint lithography (SFIL) [4]. In this technique, a resist liquid is directly dropped or dispensed on a substrate in the form of droplets with the exact amount at or near atmospheric environment (figure 1(a)). Then a mould is used, during an imprint, to push the resist droplets into a

thin film, and the liquid resist flows and merges to remove the air between the mould and the substrate (figure 1(b)). The liquid is then cured (e.g. by either photons, heat, or both) (figure 1(c)), leaving solid imprinted patterns on the substrate (figure 1(d)). One advantage of D-NIL is that it does not need vacuum, which greatly simplifies tool construction, so that vacuum operated high-precision stages (which are very hard to make and expensive) and a large vacuum chamber (which can be very bulky) are no longer needed. However, one burning key issue in D-NIL, that must be answered, is how well this method works in removing air bubbles. Namely, can the air bubbles be completely removed from the resist, and how long does it take to completely remove them? The first question is significant to the NIL quality (and hence fabrication yield) and the second to NIL throughput. Both are important to manufacturing.

In this paper, we present our experimental and theoretical study on the dynamic behaviour of air bubble formation and

³ Author to whom any correspondence should be addressed.

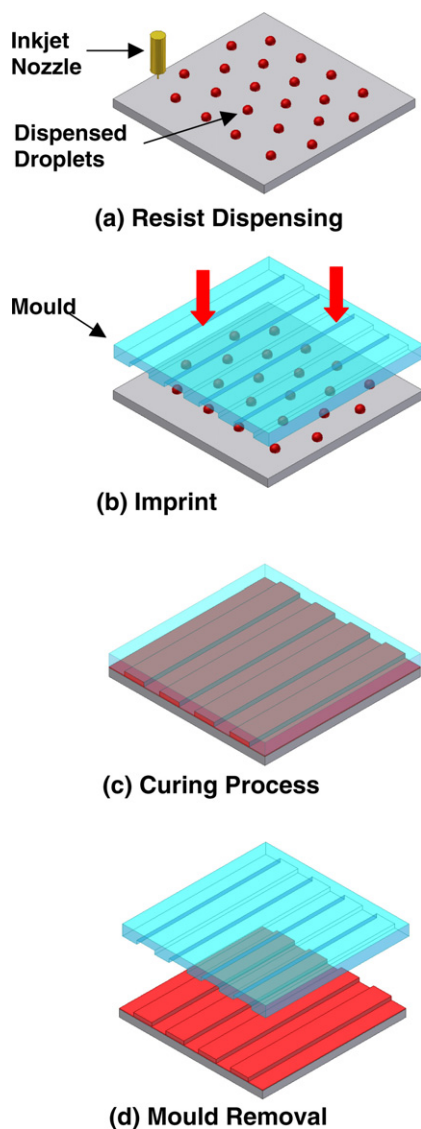


Figure 1. Schematic of dispensing nanoimprint lithography (D-NIL).

dissolution in D-NIL. This study also sheds light on other NIL methods which are performed in a poor vacuum, where air bubbles can be easily formed (e.g. NIL at atmosphere using a spin-on resist [5, 6]).

2. Two mechanisms for air bubble formation during D-NIL

Using a video camera, ink-jet dispenser, and precision stages, we observed that in D-NIL, although the spreading droplets can evacuate most air between the mould and the substrate, there are still bubbles trapped [7, 8]. We found that the bubble formation in D-NIL is due to two different mechanisms: (1) feature pinning, where liquid resist is pinned to certain surface topography and (2) encircling due to the merging of multiple droplets.

Our experiments were carried out using a Nanonex NX-3000 step-and-repeat NIL tool. An inkjet nozzle was used to dispense resist droplets with a controllable volume ranging

from 100 to 800 pl. A stage-controlled transparent mould with a 1 inch² imprint area was employed to press the resist droplets, and a digital camera was used for real-time observation of resist spreading and merging. The resist used in this work is NXR-2051 (Nanonex Corporation), which has a viscosity of 4 mPa s. For quantitative comparison between experiments and simulations, during our D-NIL experiments, the bubble area or diameter (as viewed from the top) as a function of time (i.e. dynamic behaviour) was measured by the digital camera and machine vision software of the NX-3000. Other measured parameters are the instantaneous gap size between the mould and the substrate, imprinting pressure and resist spreading area.

2.1. Feature pinning

To study the feature pinning case (figure 2), only one resist droplet of 800 pl was dispensed, which spread between the substrate and the mould that both have dense features. As shown in the schematics (figure 2(a)) and experimental observations (figure 2(b)), the spreading edge of the liquid resist pushed out the air, except at certain locations of the mould or the substrate, where the spreading edge is pinned by a feature of the surface topography while the rest of the spreading edge continuously moved forward and eventually merged, creating an air bubble behind the pinning point. After trapping, the size of the air bubble shrank with time (figure 2(b)) due to air (and vapour) absorption into the liquid resist. If an air bubble is smaller than a certain size (typically, bubble diameter $d < 100 \mu\text{m}$), the air in the bubble can be completely absorbed by the resist liquid and the bubble disappears. However, we observed that for those air bubbles with a much larger diameter (typically $d > 300 \mu\text{m}$), air in the bubble cannot be fully absorbed by the resist liquid and the bubble exists even after one hour.

Although the pinning location is unpredictable at the moment, the experiment showed that the pinning always occurred at a feature in the topology of the surface of either the mould or the substrate. The pinning topology can be in either a protrusion or concave shape with a height (or depth) ranging from several nanometres to several tens of nanometres. The size of pinned air bubbles is typically of the same order of the pattern dimension, ranging from nanometre to micrometre scales. Bubbles within this size range can be completely dissolved by liquid resists in several seconds.

2.2. Encircling of multiple resist droplets

To study air trapping by the encircling of resist droplets, multiple droplets were dispensed. The reason for NIL to use multiple droplets rather than one is to reduce the required imprinting force and increase the imprint speed [9]. However, as depicted in figure 3(a) and observed in our experiment when using four resist drops (figure 3(b)), the merging of multiple droplets encircled an air bubble at the centre of the resist layer due to the closure of air escape paths, and the bubble size reduces with time after formation. The initial air bubble size due to the multi-droplet encircling depends on the distance between the different droplets, and can be from several hundred of micrometres to millimetres. Because of their large size, these bubbles usually require a much longer time for complete dissolution and may exist for hours.

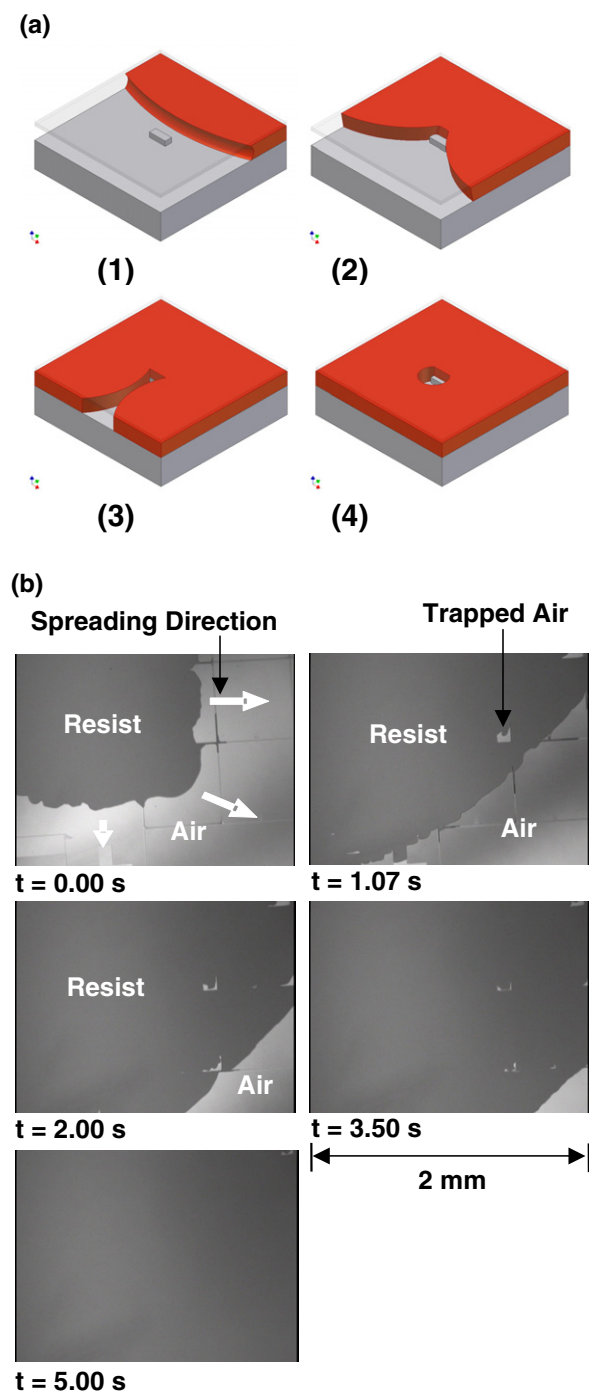


Figure 2. (a) Schematic of bubble formation due to feature trapping, and (b) real-time observation of the formation and dissolution of air bubbles when a single resist droplet is spreading between a heavily structured mould and a substrate, and air is trapped as a consequence.

For both air trapping cases, we performed a real-time study of the air bubble dissolution under different experimental conditions, such as different bubble initial size, imprinting pressure, air solubility, resist viscosity and resist residue layer thickness. The effects of imprint conditions will be discussed later to compare our observations with the theoretical model that we developed.

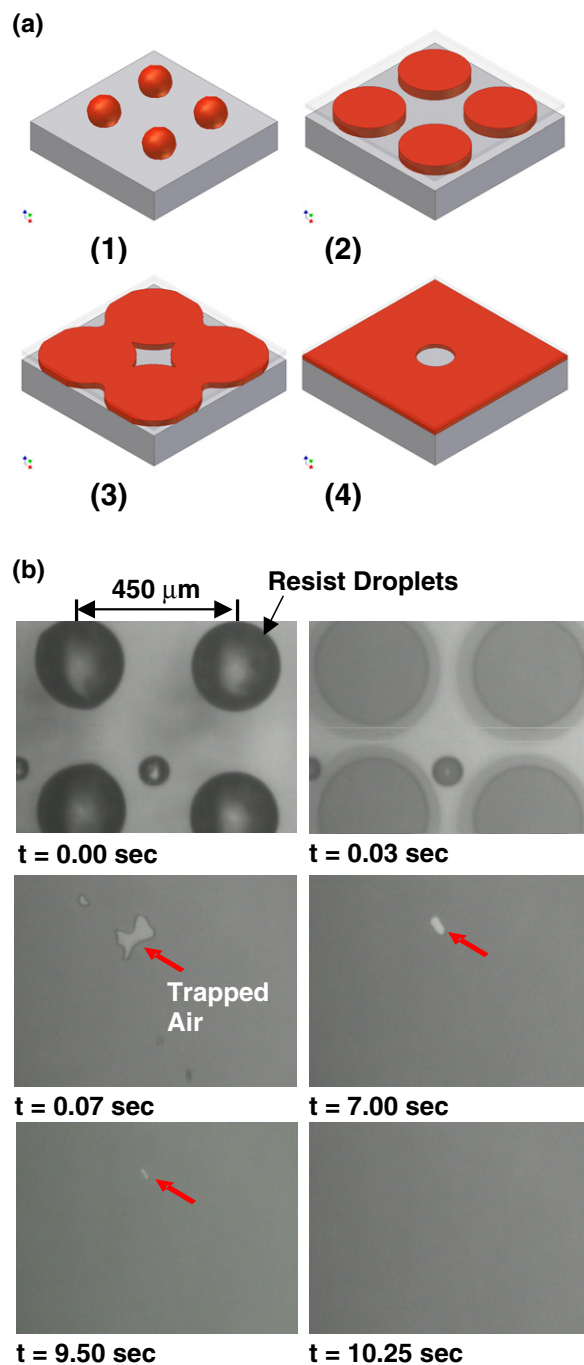


Figure 3. (a) Schematic of bubble formation due to multi-droplet encircling, and (b) real-time observation of an air bubble encircled by multiple droplets and the bubble shrinking due to the air dissolution into the resist.

3. Modelling and simulation of dynamic behaviour of air bubble

We developed a model and simulation program, based on molecular diffusion theory and hydrodynamics, to simulate the dynamic behaviour of air dissolution into the resist and the shrinkage of an air bubble. The model assumes a single air bubble trapped at the central part of an already merged

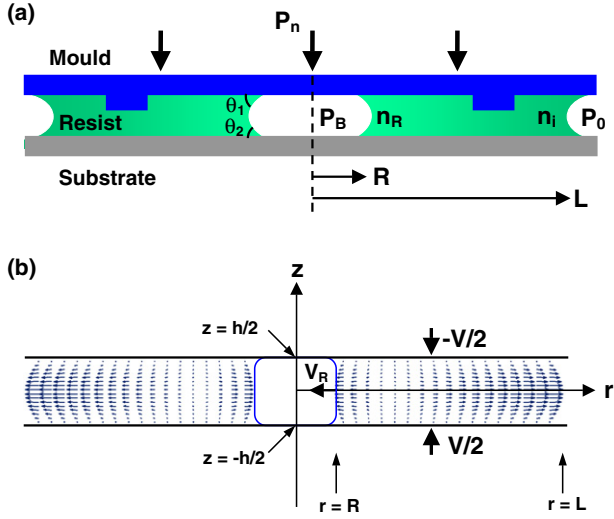


Figure 4. (a) Geometry of a single bubble surrounded by liquid resist which is pressed by an imprint mould, and (b) the illustration of the boundary conditions of flow velocity.

resist film, with the outer boundary of the resist film far away from the bubble; the fluidic flow can still be described as a Newtonian fluid; the bubble shrinking and the resist flow around the bubble are axially symmetrical; the imprinting force (and hence imprint pressure) is constant with time, which is consistent with our experimental setup; the gas trapped in the bubbles is mainly composed of air. (Our model and program could also incorporate the effects of the resist vapour and other ambient gases.) Figure 4(a) shows the geometry of the simulation model, in which a single bubble is located at the centre of a thin resist film sandwiched between a rigid mould and a substrate. During the imprinting process, the diffusion of air concentration in the resist is described by the diffusion equation (equation (1)), in which D is the diffusion coefficient of air in the liquid resist and n is the air concentration in the resist. The first and second terms on the right side of equation (1) are associated with air concentration diffusion and liquid resist flow \vec{v} , respectively [10]

$$\frac{\partial n}{\partial t} = D \nabla^2 n - \nabla \cdot (n \vec{v}). \quad (1)$$

Equation (1) can be solved subject to the following boundary and initial conditions, in which R is bubble radius; h is the thickness of the resist film; n_R is the air concentration at the bubble–resist interface; n_i is the initial air concentration in the resist; n_R and n_i are related to the bubble pressure P_B and the ambient pressure P_0 , respectively on the basis of Henry’s law (equation (2)), in which C_h is the Henry’s law constant for air dissolving into the liquid resist; parameter x is the degree of saturation of resists and typically lies between 0.9 and 1

$$\begin{aligned} n(r > R, t = 0) &= n_i \\ n(r = R, t) &= n_R \\ \lim_{r \rightarrow \infty} n(r, t) &= n_i \\ n_R &= C_h P_B \\ n_i &= x C_h P_0. \end{aligned} \quad (2)$$

Because the air bubble size changes with time, equation (1) is also coupled with hydrodynamic equations of viscous resist flow, which also must be solved. Driven by a rigid mould, the kinematics of the resist flow are satisfied by a Navier–Stokes equation with lubrication approximation (equation (3)) and the continuity equation (equation (4)), where v_r and v_z are the radial and vertical flow velocities, respectively, and μ is resist viscosity [10, 11]

$$\frac{\partial P}{\partial r} = \mu \frac{\partial^2 v_r}{\partial z^2} \quad (3)$$

$$\frac{1}{r} \frac{\partial}{\partial r} (r v_r) + \frac{\partial v_z}{\partial z} = 0. \quad (4)$$

Equations (3) and (4) are subjected to the following boundary conditions for fluidic flows, as illustrated in figure 4(b)

$$\begin{aligned} v_z \left(z = \pm \frac{h}{2} \right) &= \mp \frac{V}{2} \\ \left(2\pi r \int_{-h/2}^{h/2} v_r dz \right) \Big|_{r=R} &= 2\pi R h V_R \\ P_B &= P(R) + \sigma K_R \\ P(L) &= P_0 - \sigma K_L \\ K_R &= \frac{\cos(\theta_1) + \cos(\theta_2)}{h} + \frac{1}{R} \\ K_L &= \frac{\cos(\theta_1) + \cos(\theta_2)}{h} \end{aligned}$$

in which V is the vertical pressing velocity of the imprint mould; V_R is the shrinking rate of the bubble due to dissolution. The last two formulae in the bracket relate the pressures within the liquid resist P to the bubble pressure P_B and the ambient pressure P_0 , where σ is the surface tension; K_R and K_L are the total curvatures at the bubble–resist interface and the resist edge, respectively, and are associated with the contact angles of the liquid resist on the mould (θ_1) and the substrate (θ_2) surfaces.

The dissolution process of the air bubble based on this symmetrical configuration can be simulated by solving simultaneously equations (1)–(4) using a finite difference discretization. Table 1 lists the key parameters and symbols used in the simulation and this paper. The output data include time-dependent bubble volume or diameter, resist film thickness, bubble pressure and the instantaneous air concentration and resist flow around the shrinking bubble.

4. Experimental and theoretical results, and comparison

We simulated the air dissolution process and bubble shrinking using the same set of conditions as in our experiments, except for certain approximations as described above. In the following, we will describe both experimental and theoretical results of the dynamic behaviour of bubble dissolution (i.e. the time evolution of bubble size) and the total air dissolution time, as a function of (1) bubble initial size, (2) imprinting pressure, (3) air solubility in liquid resists (i.e. Henry’s law constant), (4) resist viscosity and (5) resist residual layer thickness (RLT).

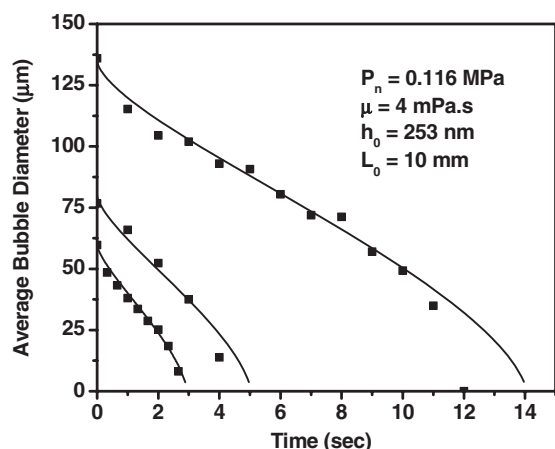


Figure 5. The simulated (—) and measured (■) time evolution of average bubble diameter as a function of bubble initial size for a given set of NIL parameters. The simulations and experiments agree well.

Table 1. Numerical values of physical parameters used in the simulations.

Physical parameters	Symbols	Value
Surface tension (N m^{-1}) ^a	σ	0.030
Resist viscosity (mPa s) ^a	μ	2–20
[12, 13] Henry's law constant ($\text{mol m}^{-3} \text{Pa}^{-1}$)	C_h	5.45×10^{-5}
Diffusion coefficient ($\text{m}^2 \text{s}^{-1}$) ^b	D	4.30×10^{-9}
Degree of saturation of the resist ^b	x	0.91
Imprint pressure (MPa) ^a	P_n	0.014–0.550
Initial resist thickness (nm) ^a	h_0	50–500
Initial resist film radius (mm) ^a	L_0	10–20
Initial bubble diameter (μm) ^a	d_i	20–800
Ambient pressure (Pa) ^a	P_0	1.01×10^5
Pressure inside the bubble (Pa)	P_B	
Shrinking rate of the bubble radius ($\mu\text{m s}^{-1}$)	V_R	
Contact angles ^a	θ_1, θ_2	$45^\circ, 30^\circ$

^a Experimentally measured values.

^b Fitting parameters.

4.1. Effects of initial air bubble size

Figure 5 shows experimental and simulated dynamic behaviour of air bubble size as a function of the bubble initial size for a given set of NIL parameters (i.e. imprinting pressure, viscosity, resist initial thickness and spreading area). The simulations agree well with the experiments, indicating the model and simulation programs are valid. The only fitting parameters in the simulation are the diffusion coefficient of air in the resist D and the degree of saturation of the resist x (see table 1). Clearly, the experiments and simulations show that the total air dissolution time in resist strongly depends upon the bubble initial size. Typically tens of seconds are required to dissolve a $100 \mu\text{m}$ diameter bubble, and 160 s for a 1 mm bubble. Note that the total air dissolution time can be much longer if imprint pressure is lower or the resist residue layer thickness is thinner, as discussed below in sections 4.2 and 4.5.

The dynamic behaviour in figure 6 indicates that the air bubble size decreases with time almost linearly (i.e. constant air dissolution rate) except near the end. This is due to

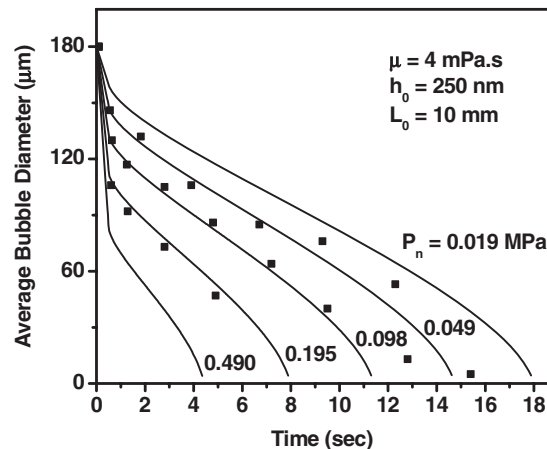


Figure 6. The simulated (—) and measured (■) time evolution of average bubble diameter as a function of the imprinting pressure.

the fact that a constant imprinting pressure makes the bubble pressure nearly constant, which leads to a relatively constant air concentration at the bubble–resist interface (Henry's law) and hence a relatively constant dissolution rate. The deviation from a constant dissolution rate at the end of air absorption is caused by small bubble diameters, which will introduce a sizable Laplace pressure that accelerates air absorption.

4.2. Effects of imprinting pressure

Imprinting pressure plays an important role in D-NIL. The increase of the imprinting pressure can accelerate not only the spreading and merging of the resist droplets but also the air dissolution rate. Figure 6 shows the simulation and experimental results of the imprinting pressure effects on the dynamic behaviour of air dissolution and bubble shrinking. Again the simulations and experiments agree well with each other. For an air bubble with a given initial average diameter of $180 \mu\text{m}$ and a given resist initial thickness of 250 nm , an increase of imprinting pressure from 0.019 to 0.49 MPa (~ 20 times) can reduce the air bubble shrinking time from 18 to 4.2 s (~ 4.5 times). The reason for the faster dissolution rate (hence a shorter total dissolution time) at a higher imprinting pressure is that a higher imprinting pressure gives a larger air concentration at the bubble–resist interface n_R (according to Henry's law (equation (2))), which in turn gives a higher dissolution rate (equation (1)). However, an excessively high imprint pressure has the drawbacks of poor overlay alignments, and the potential of damage to the mould and substrate.

The dynamic behaviour in figure 6 shows that, as the imprinting pressure becomes higher, the air bubble size first quickly reduces to a smaller size, which is according to Boyle's law (here, we assume that all bubbles have the same initial size at the same pressure), and then the bubble gradually shrinks due to air dissolution.

4.3. Effects of air solubility (Henry's constant)

Another potential way for accelerating the bubble dissolution is to increase the air solubility in the resist, which is characterized by the Henry's law constant C_h . For a given bubble pressure, the larger Henry's constant leads to the higher air concentration

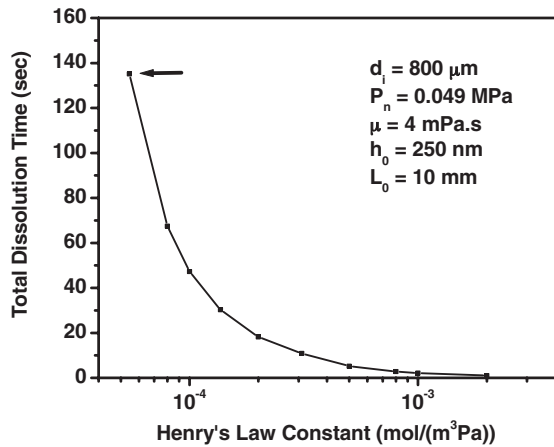


Figure 7. The simulated total dissolution time as a function of the Henry's law constant for an 800 μm diameter bubble under a typical NIL condition.

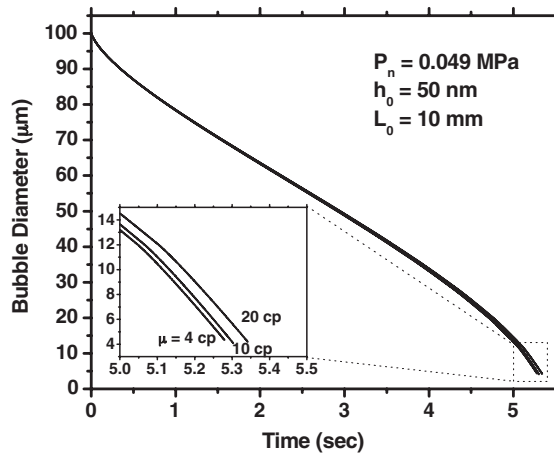


Figure 8. Simulated time evolution of bubble diameter as a function of the resist viscosity.

at the bubble–resist boundary (see equation (2)), which can increase the air dissolution rate into the liquid. Figure 7 plots the simulated total dissolution time as a function of the Henry's law constant for a given bubble initial size ($d_i = 800 \mu\text{m}$) and a set of typical NIL parameters. It shows that the total dissolution time is inversely proportional to Henry's law constants approximately. For example, if Henry's constant C_h is increased from $5.5 \times 10^{-5} \text{ mol m}^{-3} \text{ Pa}^{-1}$ to $3.0 \times 10^{-4} \text{ mol m}^{-3} \text{ Pa}^{-1}$, the time for completely dissolving this 800 μm bubble could be reduced from 135 to 10 s. If $C_h > 2.0 \times 10^{-3} \text{ mol m}^{-3} \text{ Pa}^{-1}$, this dissolution time could be less than 1 s. Hence, liquid resists with higher air solubility can be more effective in reducing the bubble dissolution time.

4.4. Effects of resist viscosity

In principle, a lower resist viscosity can lead to a shorter bubble dissolution time because of the less viscous resistance to oppose the shrinking movement of the bubble–resist boundary. However, in reality, we found that this reduction of bubble dissolution time is small. Figure 8 shows our simulation of dynamic behaviour of the bubble dissolution

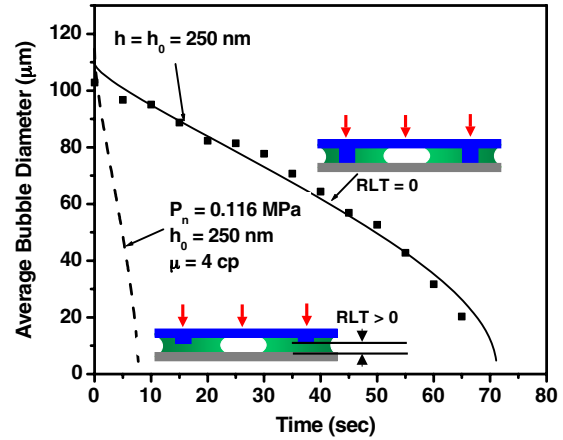


Figure 9. The simulated (---) and measured (■) time evolution of average bubble diameter for the case of RLT = 0. In comparison with the case of RLT > 0 (---), it is indicated that, when RLT is close to zero (or a critical thickness), the bubble dissolution rate can be significantly reduced, and the total dissolution time increases.

as a function of resist viscosity. As the viscosity increases from 4 to 20 mPa s⁻¹ (typical values for D-NIL) the simulated dissolution time of a 100 μm diameter bubble increases only by about 1%. This can be explained as following: the bubble pressure, which directly controls the dissolution rate (see equation (2)), is the sum of the contributions from imprinting pressure, Laplace pressure, and viscous stress. However, based on our numerical simulation, for an air bubble trapped in a thin resist film (typically $h_0 < 300 \text{ nm}$), the viscous stress induced by the bubble shrinking is smaller than the bubble pressure by about two orders of magnitude, therefore leading to a very limited effect on the air dissolution rate.

4.5. Effects of resist residual layer thickness

The residual layer thickness (RLT), measured as the final gap between the mould protrusion and the substrate surface (see insets in figure 9), is another factor that can significantly affect the air dissolution time. In the previous discussion, we have assumed the RLT is thick. However, when RLT becomes zero (i.e. the mould protrusion and the substrate are brought into direct contact) or nears zero, the substrate stops the mould movement and balances the imprinting pressure on the mould, and hence the mould will not press the liquid further, and pressure in the liquid can be much less than the imprint pressure. Therefore, after RLT become zero, the air dissolution becomes much slower, leading to a longer total air absorption time. Figure 9 shows the simulated and experimental dynamic behaviours of bubble dissolution, respectively, in the case of RLT = 0. For comparison, the case of RLT > 0 was also simulated considering the identical NIL conditions (dashed line in figure 9). It shows that the total air dissolution time for RLT = 0 is about 10 times longer than that for RLT > 0. In reality, when the resist RLT is reduced to a thickness where the local viscous friction is equal to or greater than the imprinting force, the resist cannot be squeezed out from the residual layer, and the mould stops moving. In this case, the pressure outside the residual layer is much less than the average imprinting pressure, and the situation can also be approximately regarded as RLT = 0.

5. Impact on NIL yield and throughput

From our experimental and theoretical study of D-NIL operated in or near atmosphere, it is clear that air bubbles can be dissolved in the resist, but the dissolution process may take time given in minutes or even hours. This poses serious challenges to the yield and throughput of D-NIL. The study reported here identifies the key factors affecting the air bubble dissolution rate and provides guidelines for reducing the air dissolution time. Based on our study, the total dissolution time of an air bubble can be significantly reduced by decreasing the bubble initial size or increasing the imprinting pressure and resist Henry's law constant. For the air bubble trapped in a thin resist film (typically $h_0 < 300$ nm), the resist viscosity does not play an important role in bubble dissolution. When the resist residual layer thickness is close to zero or a critical thickness, the bubble dissolution process can be significantly slowed down.

Acknowledgments

This work was supported in part by the Office of Naval Research (ONR) and the Defense Advanced Research Projects Agency (DARPA).

References

- [1] Chou S Y, Krauss P R and Renstrom P J 1995 *Appl. Phys. Lett.* **67** 3114
- [2] Chou S Y, Krauss P R and Renstrom P J 1996 *Science* **272** 85
- [3] Chou S Y, Krauss P R, Zhang W, Guo L and Zhuang L 1997 *J. Vac. Sci. Technol. B* **15** 2897
- [4] Kim E, Xia Y and Whitesides G M 1995 *Nature* **376** 581
- [5] Colburn M, Johnson S, Damle S, Bailey T, Choi B, Wedlake M, Michaelson T, Sreenivasan S V, Ekerdt J and Willson C G 1999 *Proc. SPIE* **3676** 379
- [6] Haisma J, Verheijen M and Heuvel K V D 1996 *J. Vac. Sci. Technol. B* **14** 4124
- [7] Liang X G, Zhang W, Li M T, Xia Q F, Wu W, Ge H X, Huang X Y and Chou S Y 2005 *Nano Lett.* **5** 527
- [8] Liang X G, Fu Z L and Chou S Y 2005 *Proc. 4th Int. Conf. on Nanoimprint and Nanoprint Technology (Nara, Japan, Oct. 2005)*
- [9] Reddy S and Bonnecaze R T 2004 *Proc. 3rd Int. Conf. on Nanoimprint and Nanoprint Technology (Vienna, Austria, Dec. 2004)*
- [10] Colburn M, Choi B J, Sreenivasan S V, Bonnecaze R T and Willson C G 2004 *Microelectron. Eng.* **75** 321
- [11] Landau L D and Lifshitz E M 2003 *Fluid Mechanics* 2nd edn (Oxford: Butterworth-Heinemann)
- [12] Reynolds O 1886 *Phil. Trans. R. Soc.* **177** 157
- [13] Teodorescu M, Persson O and Rasmussen P J 2001 *Chem. Eng. Data* **46** 640
- [14] Hirose T, Mizoguchi K and Kamiya Y J 1985 *Appl. Polym. Sci.* **30** 401